2022

Rotordynamic and Fatigue Analyses of a Twin-Screw Compressor with 4-6 Configuration and Internal Cooling Channels

Abhignan Saravana

Haotian Liu

Nicholas Able

James Collins

Eckhard A. Groll

See next page for additional authors

Rotordynamics and Fatigue Analyses of a Twin-Screw Compressor with 4-6 Configuration and Internal Cooling Channels

Abhignan SARAVANA[(1)]*, Haotian LIU[(1)], Nick ABLE[(2)], James COLLINS[(2)], Eckhard A. GROLL[(1)], Davide ZIVIANI[(1)]

[(1)] Ray W. Herrick Laboratories, School of Mechanical Engineering, Purdue University
West Lafayette, 47907-2099, USA
saravan0@purdue.edu; liu1460@purdue.edu; groll@purdue.edu; dziviani@purdue.edu

[(2)] Ingersoll Rand
Nicholas_Able@irco.com; James_Collins@irco.com

* Corresponding Author

ABSTRACT

Twin-screw compressor technology is widely employed in commercial and industrial HVAC&R applications as well as in air-compression and gas processing industries. Twin-screw compressors are characterized by relatively high efficiencies at part and full-loads, and high reliability. However, innovative designs and higher efficiency are needed to further reduce power consumption, improve the compression process, and minimize internal losses.

This study focuses on the development of a hollow twin-screw compressor with internal cooling channels to achieve a near isothermal compression process. Over time, the rotors can be affected by stress accumulation and deformations due to their hollowness and reduced wall thicknesses. To analyze the dynamic behavior of the rotor pair, a detailed rotordynamic simulation model and a fatigue analysis have been conducted by using the actual compression forces obtained from previous CFD studies. Both hollow and solid rotors have been analyzed and compared. The bearing loads have been verified against Campbell diagrams whereas the fatigue results have been compared with experimental testing. With the validated model, the hollow rotor compressor durability was analyzed and compared with the conventional rotors.

1. INTRODUCTION

Twin-screw compressors are positive displacement machines that are widely used in gas compression for various applications due to their high efficiency and reduced number of moving parts (Patel and Lakhera, 2019). The working principle of twin-screw compressors relies on the gearing of female and male screw rotors that creates flute-type working chambers that decrease in volume from suction to discharge (Stosic *et al., 2005*). Based on the lobe configurations and operating conditions, the rotors are subjected to radial and axial compression loads that ultimately must be compensated by means of bearings. Therefore, to ensure reliable operation, rotordynamics, rotor deflection and fatigue analysis are important aspects to be considered while optimizing the screw compressors.

In the literature, several studies can be found on computing twin-screw compression forces and moments and estimating the bearing loads. For instance, Zhou *et al*. (1990) presented a simplified method to compute compression loads by resolving pressure loads into axial forces and radial forces acting on various sections of the geometry. However, the model did not account for the pressure loads varying along the compression chamber and assumed a common pressure load acting evenly on the rotor, therefore sacrificing the accuracy of the results. Adams (1997) developed a more accurate method to compute bearing loads through an analytical approach by using pressure vs. surface area curves developed by projecting the 3D rotor surface onto 2D planes. Lee (1999) proposed a mathematical model to simulate the behavior of the twin screw air compressor and compute the compression loads using rotor groove profiles. This method follows the method outlined by Adams (1997) but uses rotational coordinates. Wu *et al.*

(1995) provides a FEM method to calculate bearing loads using a 3D approach. The pressure loads were computed using finite element analysis and the forces were verified by an experimental setup for the same working conditions.

Literature has been quite on the rotordynamic aspect of twin-screw compressors. However, there has been progress done on rotordynamics of twin-screw pumps (Muhammad and Childs, 2013). The study employed a 3D finite element method approach to analyzing rotordynamics in twin-screw pumps by representing the screw rotor geometry using axisymmetric beam elements and predicts the static and dynamic lateral forces from the unbalanced pressure loads. It discusses both transience and steady state conditions for twin-screw pumps.

This paper focuses on the FEA approach to resolving bearing loads and calculating stresses over the rotor using only a stationary, steady state approach. The compressor used in this study is manufactured using direct metal laser sintering and the geometry is unconventional. To reduce the temperature effects and overheating of a conventional twin-screw compressor, internal cooling channels to achieve a near isothermal compression process are engraved inside the rotor making it hollow. The thinner rotor surfaces present a new challenge for stress accumulation and hence the need for evaluating rotor stresses. This paper presents a rotordynamic simulation conducted on the modified twin screw compressor and uses this result in a fatigue analysis to compute the factor of safety. The simulation is verified with a conventional rotor setup using rotordynamic frequency responses.

2. TWIN SCREW COMPRESSOR MODEL

The twin-screw compressor modeled in this paper is a 4-6 configuration with an internal channel for coolant flow. The working fluid is air, and the coolant is water. The male and female rotors are both additively manufactured out of Inconel. There are three sub-models: the geometry model describes the modified geometry of rotors to accommodate the internal fluid domain, the stationary domain rotordynamic model used for FEA and the fatigue models used to calculate appropriate factor of safeties. The general model descriptions and specific model modifications and improvements are briefly described in this section.

2.1 Geometry model

As previously mentioned, the original geometry of the rotors was modified to include an internal fluid domain, thus making them hollow. The original structure of the rotors was scaled down and transformed into a wavy pattern to maximize convective heat transfer to the coolant. This hollow fluid domain is later engraved into the original geometry, thus creating a pocket. The wavy transformation is created based on a parametric profile derived by tracing the outer perimeter of the rotors. Figure 1 describes this procedure on the male rotor. The wavy internal profile is scaled down at an offset of 5mm from the outer male rotor geometry.

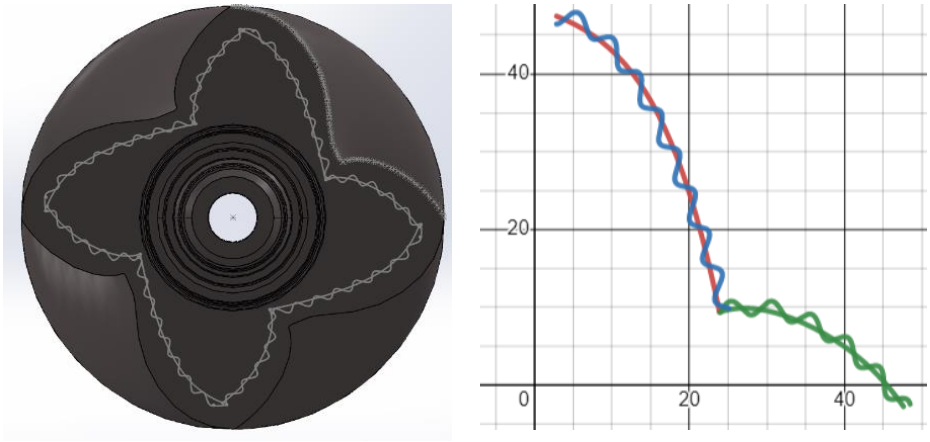

(a) **(b)**

Figure 1 Male rotor with internal cooling channel: a) 2D view of male rotor with internal fluid domain projections; b) male rotor profile with wavy transformation

The geometry is split into two parametric sections, described by the red and green curves as shown in Figure 1(b). Figure 1(b) also illustrates how the wavy transformation overlaps the initial profile. A similar procedure was repeated for the female rotor as well. The below equations describe the parametric form of the wavy internal geometry. The parameters *m* and *a* are optimized to produce a perfect overlay of the wavy over the smooth profile. The wavy projections are then patterned around the circumference of the rotors to resemble the other lobes.

$$x_t = \left(t + a * t * \frac{cos\left(m*t*sqrt\left(1+(a*t)^2\right)\right)}{sqrt(1+(a*t)^2)} \right) \quad (1)$$

$$y_t = \left(a * t^2 - \frac{cos\left(m*t*sqrt\left(1+(a*t)^2\right)\right)}{sqrt(1+(a*t)^2)} \right) \quad (2)$$

This 2D projection is wrapped around the length of the rotors using a helix spiral whose parameters are based on the rotor geometry. The initial angle of the helix is at the start point of the fluid domain and wrapped around the length of the rotor using basic pitch and wrap angle calculations. The final rotor geometries are displayed in Figure 2.

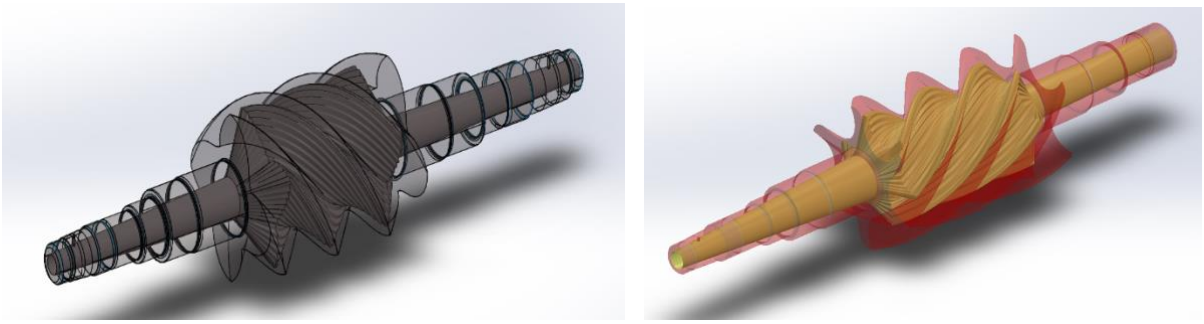

Figure 2: CAD model of male (left) and female (right) rotors with internal fluid domain projections

2.2 Rotordynamics Model

To study the rotordynamics of both male and female rotors, boundary conditions and loads from the CFD simulations have been used. A steady-state approach has been used to impose the loads on the rotors. The maximum and minimum value of pressure loads, derived from CFD were used as the constant loads for two different cases. These two cases were later used in the fatigue model as two alternating max and min cases.

The stationary model operates on a co-rotating reference frame. Due to this modeling strategy, it does not involve the acceleration and time effects otherwise seen on a stationary reference frame. The frame setup is depicted in Figure 3.

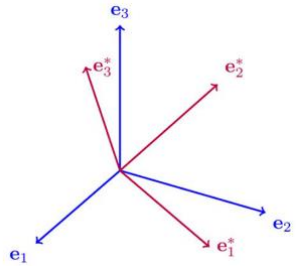

Figure 3: Canonical basis in stationary frame setup vs co-rotating frame setup (asterisk)

A vector can be transformed from one basis to the other using a transformation matrix R via the following relations,

$$v = v.(e_i)e_i = v_i e_i \quad (3)$$

$$e_i^* = (e_i^*.e_j)e_j = R_{ij}e_j \quad (4)$$

$$v_i^* = v.e_i^* = v.\left(R_{ij}e_j\right) = R_{ij}v_j \tag{5}$$

Both coordinate systems have reference zeros independent from each other and these are represented by $\mathbf{x_s} = 0$ and $\mathbf{x_r}^* = 0$. Therefore, the following relations exist between the space-fixed coordinate **x** and the co-rotating geometry-fixed coordinate $\mathbf{x}^*$.

$$x = R^T(x^* - {x_s}^*) \tag{6}$$
$$x^* = R(x - x_r) \tag{7}$$
$$x_r = -R^T x_s^* \tag{8}$$
$$x_s^* = -Rx_r \tag{9}$$

If $\mathbf{X_{bp}}$ is the base point of rotor axis in space-fixed frame which defines the origin of the corotating frame, the position of any arbitrary point X in the corotating frame is,

$$X_r = X - X_{bp} \tag{10}$$

Therefore, the position vector of particle at X after deformation ($\boldsymbol{\chi}$) in the space-fixed frame is,

$$\chi(X,t) = X_{bp} + R(X_r + u_r) = X_{bp} + R(X + u_r - X_{bp}) \tag{11}$$

where the rotation matrix **R**, that transforms components in the rotational frame to the fixed frame, which is defined as,

$$R = cos\theta \boldsymbol{I} + \frac{\sin\theta}{\theta}(\boldsymbol{\theta} \times \boldsymbol{I}) + \frac{1-cos\theta}{\theta^2}(\boldsymbol{\theta} \otimes \boldsymbol{\theta}) \tag{12}$$

where θ is the magnitude of rotation matrix $\boldsymbol{\theta}$ and **I** is the identity matrix and $\otimes$ stands for the dyadic product. The total displacement of any point on the rotor including rotational effects expressed in the fixed frame is,

$$u = \chi(X,t) - X = Ru_r + (R - I)(X - X_{bp}) \tag{13}$$

Differentiating the displacement term twice, yields to acceleration in the space-fitted frame,

$$\frac{\partial \chi(\mathrm{X,t})}{\partial t} = \frac{\partial \mathrm{R}}{\partial t}\left(X + u_r - X_{bp}\right) + R\left(\frac{\partial \mathrm{u_r}}{\partial t}\right) = R[\widetilde{\Omega_\mathrm{r}}\left(X + u_r - X_{bp}\right) + \left(\frac{\partial \mathrm{u_r}}{\partial t}\right)] \tag{14}$$

$$\frac{\partial^2 \chi(\mathrm{X,t})}{\partial t^2} = Ra_r = R[(\frac{\partial \widetilde{\Omega_\mathrm{r}}}{\partial t} + \widetilde{\Omega_\mathrm{r}^2})\left(X + u_r - X_{bp}\right) + 2\widetilde{\Omega_\mathrm{r}}\left(\frac{\partial \mathrm{u_r}}{\partial t}\right) + \frac{\partial^2 \mathrm{u_r}}{\partial t^2}] \tag{15}$$

Where $\widetilde{\Omega_\mathrm{r}}$ represents angular velocity. The total acceleration in the rotating frame is therefore given as,

$$a_r = R[(\frac{\partial \widetilde{\Omega_\mathrm{r}}}{\partial t} + \widetilde{\Omega_\mathrm{r}^2}) \times \left(X + u_r - X_{bp}\right) + 2\widetilde{\Omega_\mathrm{r}} \times \left(\frac{\partial \mathrm{u_r}}{\partial t}\right) + \frac{\partial^2 \mathrm{u_r}}{\partial t^2}] \tag{16}$$

For support locations on the rotor, the X_r in equation for $\chi(X,t)$ is replaced by X_{ax} where X_{ax} is given by,

$$X_{ax} = X_1 + [(X - X_1).e_1]e_1 \tag{17}$$
$$e_1 = \frac{X_2 - X_1}{abs(X_2 - X_1)} \tag{18}$$

where X_1 and X_2 represent the position vectors on the rotor that represent the two support locations which are used to define the axis of rotation about which the rotors rotate. For the stationary analysis, the acceleration a_r reduces to,

$$a_r = \widetilde{\Omega_r^2} \times \left(X + u_r - X_{bp}\right) \tag{19}$$

2.3 Fatigue Model

The Findley criterion was used to estimate the factor of safeties based on the stationary rotordynamic models. The basic theory for the Findley criterion (Svärd 2014) is stated below,

$$\left(\frac{\Delta\tau}{2} + k\sigma_n\right)_{max} = f \tag{20}$$

where k and f are material parameters, $\Delta\tau$ is the maximum shear stress range on a plane, and σ_n is the largest normal stress on the same plane. The plane that maximizes the left-hand side of the equation is critical. Hence, the fatigue usage factor f_{us}, also known as the inverse of factor of safety, is computed with the following,

$$f_{us} = \frac{\left(\left(\frac{\Delta\tau}{2} + k\sigma_n\right)_{max}\right)}{f} \tag{21}$$

The two material properties k and f are experimentally obtained using a fatigue test with two different loading conditions, which can be either pure torsion or pure tension. The calculation of f and k through these conditions is described using the following equations,

$$\sqrt{\left(\frac{\sigma_{max} - \sigma_{min}}{2}\right)^2 + (k \cdot \sigma_{max})^2} + k.\sigma_{max} = 2.f \tag{22}$$

$$\tau_a = \frac{f}{\sqrt{1+k^2}} \tag{23}$$

where σ_{max} and σ_{min} are the maximum and minimum stresses at the fatigue limit (i.e. infinite life), respectively.

3. SIMULATION SETUP

3.1 Rotordynamics setup

Several considerations and assumptions were made to setup the simulations. Appropriate boundary conditions, material properties, bearing placement and loading setup were carefully assessed to ensure a representative case study with respect to the real compressor assembly. The rotordynamics and fatigue setup were done individually and separately for each of the male and female rotors. The geometry setup consisted of the rotor and the roller bearing for containing radial forces as that was the focus within the study. The geometry for both male and female rotors with the bearings setup is displayed in Figure 4.

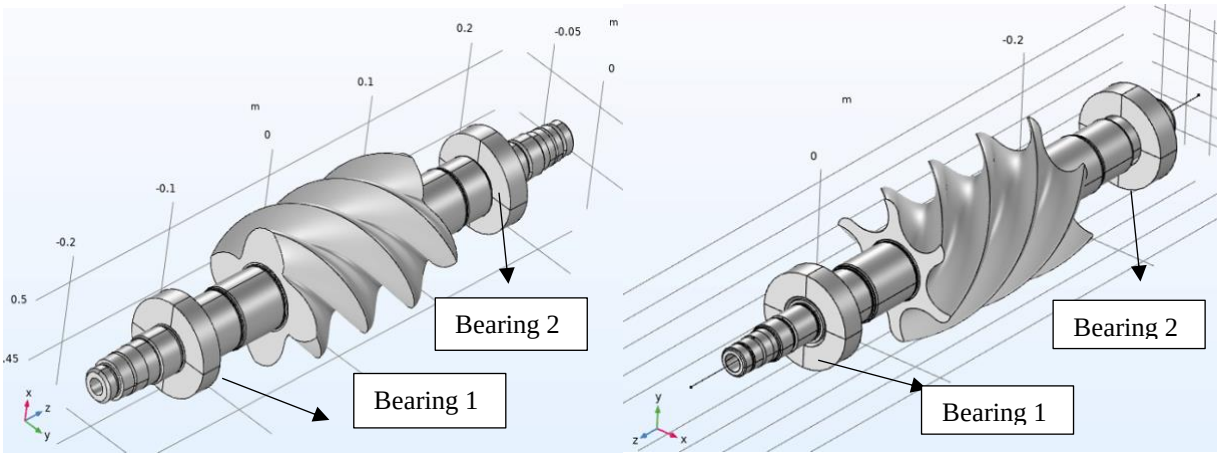

Figure 4: Isometric view of male (left) and female (right) with the radial cylindrical roller bearings assembled

The axis of rotation was setup by defining two locations on either side of the rotor. The axis is then defined by a line drawn connecting these two locations as described in the previous section. An example of the two locations for the female rotor is show in Figure 5. The same is repeated on the male rotor.

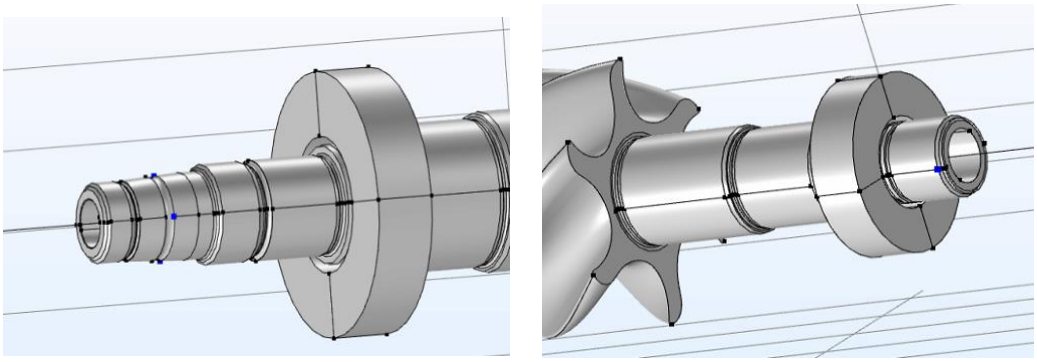

Figure 5: Support locations defined on the bearing 1 and 2 of the female rotor respectively

The boundary load consists of two pressure loads that only act on the rotor surface: whose values equal to the maximum and minimum values of pressure load variation from an external CFD study. These contribute to two load cycles which are fed as boundary conditions in the fatigue setup. The bearings are modeled using a flexible platform type analysis whose damping coefficient, stiffness values and other bearing properties are summarized below in Table 1 and Table 2. These damping and stiffness coefficients were obtained experimentally.

Table 1: Bearing setup

Bearing	**Young's modulus (GPa)**	**Poisson's ratio (-)**	**Diameter (m)**		**Height (m)**	**Stiffness constants**		**Damping Coefficients**	
			Inner	**Outer**		K_u $\left(\frac{\mathrm{N}}{\mathrm{m}}\right)$	K_θ $\left(\frac{\mathrm{N\,m}}{rad}\right)$	C_u $\left(N\frac{s}{m}\right)$	C_θ $\left(\mathrm{N\,m}\frac{s}{rad}\right)$
Female rotor cylindrical roller	200	0.3	0.03	0.062	0.016	175,000	1	7,000	0
Male rotor cylindrical roller	200	0.3	0.035	0.072	0.017	175,000	1	7,000	0

Table 2: Rotor bearing specifications

Rotor	**Number of rollers**	**Roller diameter (m)**	**Roller length (m)**	**Pitch diameter (m)**	**Radial clearance (m)**
Female	13	0.009	0.01	0.046	0.0002
Male	14	0.01	0.011	0.0535	0.0002

3.2 Fatigue setup

The two different cases consisting of P_{max} and P_{min} for male and female rotors each are used as load cycles in the fatigue setup. The other parameters of the Findley criterion were selectively chosen based on experimental research and available knowledge of the material.

The endurance limit or infinite life fatigue limit of additively manufactured Inconel was determined to be 275 MPa, through externally conducted rotational beam testing. The other factor *k* was chosen to be around 1.5, which was determined to be conservative for this application.

4. RESULTS AND DISCUSSION

The rotordynamic model in COMSOL Multiphysics (Inc. C., 2020) is verified using a 1D approach. The Campbell plots for both the cases have been compared with the experimental data and the error propagation is discussed in this section.

4.1 Model Verification

The simulation setup, including boundary conditions, was validated by generating Campbell plots using an eigenfrequency study (Lee, C.-W., & Seo, Y. H., 2009) & (Kliemann, Wolfgang, & Namachchivaya, N. S., 2017). The Campbell plots from the simulation were compared to that of a numerical 1D model for three different cases: the hollow female rotor with no load, hollow female rotor with load, hollow male rotor with load. The comparisons between experimental and numerical results are displayed in Figure 6.

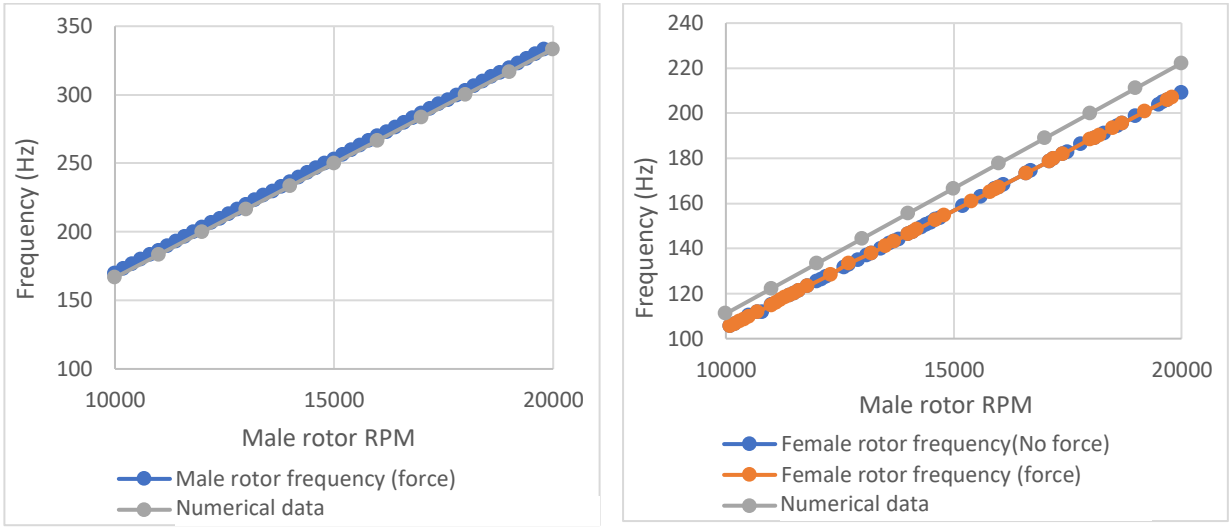

(a) Male Rotor **(b) Female Rotor**

Figure 6: Comparison of Campbell plots for (a) male and (b) female rotors with and without load over that obtained through the numerical model

As the Campbell plots are not affected by the loads and are truly dependent on geometrical factors such as stiffness and damping coefficients, they validate the simulation setup with numerically obtained results from the 1D model. From Figure 6, it can be observed that the simulation model underpredicts eigenfrequencies for the same range of rotor operating speeds for the female rotor with an average error of 6.2%. This pattern, however, isn't the same for the male rotor as the error is significantly lower with an average of 1.2%. It can also be observed that the female rotor frequencies with and without loads are similar; this proves the earlier argument that the Campbell plots are not affected by loads and are dependent on geometry and rotational speeds. It can be concluded that the simulation is valid and precise, while the accuracy is within an acceptable range.

4.2 Stress Analyses

The main purpose of this paper is to calculate the stationary von Misses stresses acting on the male and female rotors using rotordynamics and use this result to compute respective factor of safeties and conclude the area of maximum stress. As the stationary pressure loads only act perpendicular to the rotor surface area, it can be predicted that the stress concentrations occur along the rotor surface area. These pressure loads when reversed between maximum and minimum load cycles, as explained in earlier sections, can cause prominent fatigue effects on these areas due to repeated loading. Because the rotor surface areas incur the maximum amount of stress, lower factor of safeties are concentrated on these areas. These arguments are corroborated through contour plots depicted in Figure 7.

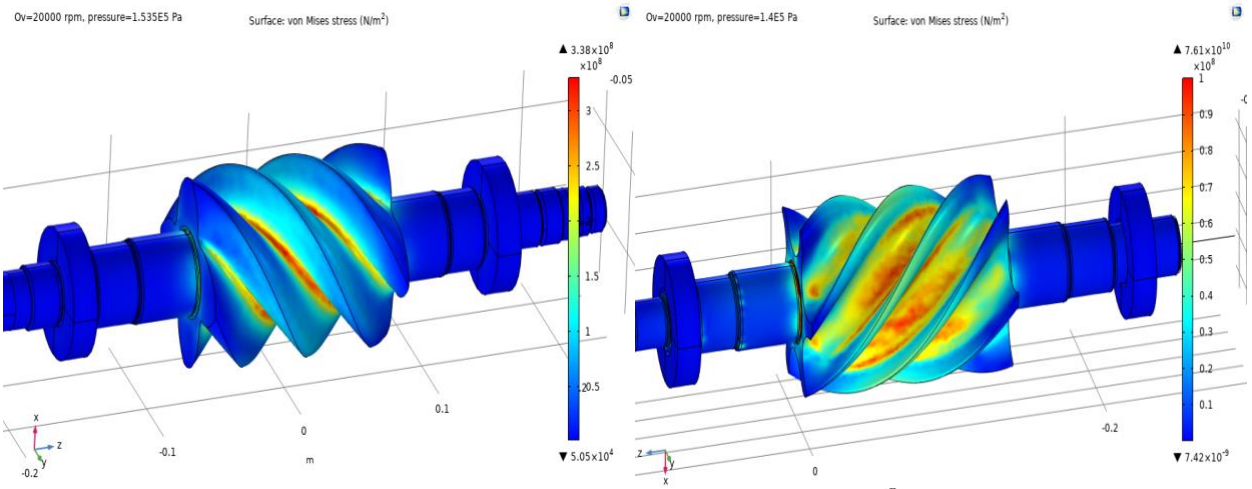

Figure 7: Von Misses stress contour plots on male (left) and female (right) rotors respectively

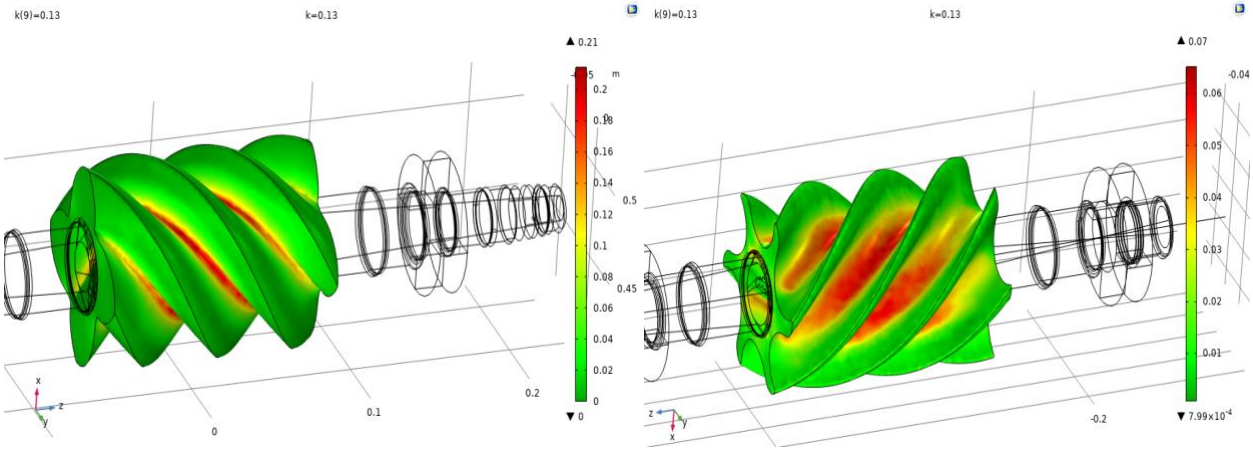

Figure 8: Fatigue usage factor (i.e. reciprocal of factor of safety) for male (left) and female (right) rotors, respectively

The stationary von Misses stress plots in Figure 7 display stress values for a male rotor rotation speed of 20,000 RPM for both male and female rotors. It must be noted that due to the gear ratio of 4-6, the female rotor rotates at a much slower rotation speed. The results displayed are for the maximum pressure load cycle, therefore these are the maximum stresses occurring on the rotors at the operating conditions they are designed for. Figure 8 describes the fatigue usage factor (***f***) distribution across the rotors for the same operating conditions; *f* can be equal to inverse of factor of safety.

As it was earlier discussed, the stress points occur along the rotor surface area. The stresses are larger for the male rotor, as can be expected due to the higher male rotor rotational speed. Because of this, a maximum fatigue usage factor of 0.2 occurs on the male rotor. This is equivalent to a factor of safety of 5. Through the above results, it can be concluded that through the factor of safety calculations, the modified twin-screw compressors can be safely operated under the design conditions.

The simulation results can also be applied to investigate the radial loads on the bearings for both rotors. As can be concluded from Figure 9, the male rotor has to endure a higher amount of bearing load as compared to the female rotor. Since the male rotor has a higher rotational speed and higher pressure load, this result can be justified. The maximum radial force magnitudes are 94.7 N and 476 N on the female and male rotors respectively.

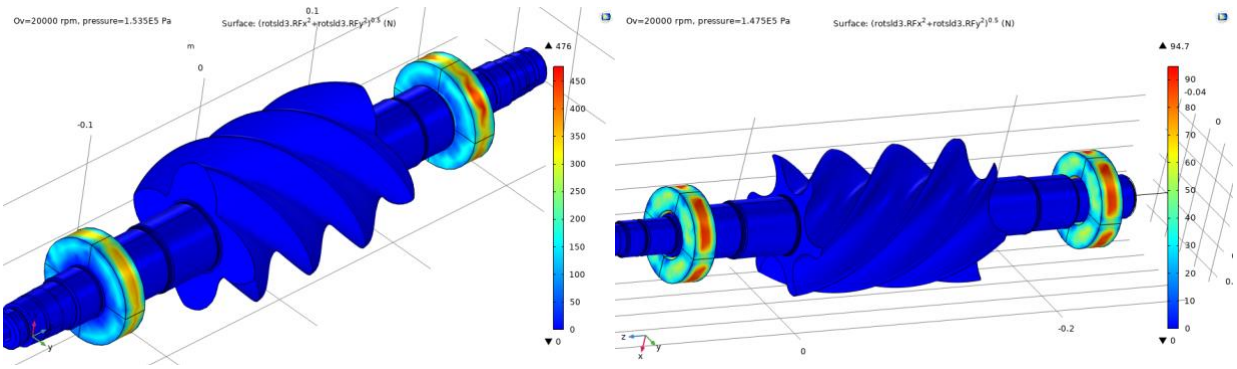

Figure 9: Bearing loads on male (left) and female (right) rotors

5. CONCLUSIONS

In this paper, a comprehensive rotordynamics model of a 4-6 configuration twin-screw compressor has been presented and verified. A stationary domain approach is used to compute rotordynamic von Misses stresses. These stresses are used to compute fatigue factor of safeties using the Findley criterion. The model and geometry setup has been verified through Campbell diagram plots compared to that of a numerical model. The model predictions show good agreement (within 6%) for both male and female rotors. The rotordynamic von Misses stresses are maximum on the male rotor, thus leading to lower factor of safeties occurring on the rotor surfaces. These are however within range and therefore concluded to be safe to use. Further investigation of the complete bearing setup with gears can further improve the models accuracy by computing stress values.

NOMENCLATURE

e	canonical basis vectors	
v	any vector in a basis	
R	transformation matrix from stationary to rotational frame	
x	any point in the spatial coordinate system	
x^*	same point in the rotational coordinate system	
X_{bp}	base point of rotor axis in space-fixed frame	
X	any arbitrary point in the space-fixed frame	
X_r	any point observed in the rotating frame	
χ	any point X after deformation in the space-fixed frame	
u_r	displacement of point x in the rotating frame	
$\boldsymbol{\theta}$	rotation vector	
θ	magnitude of rotation vector	
$\mathbf{I}$	identity matrix	
t	time	s
$\widetilde{\Omega_r}$	angular velocity tensor	$\mathrm{rad/s}$
a_r	acceleration in rotating frame	rad/s^2
$\Delta\tau$	maximum shear stress	Pa
k	normal stress sensitivity coefficient	–
f	fatigue limit (i.e. endurance limit)	Pa
f_{us}	fatigue usage factor	–
k	normal stress sensitivity coefficient	–
σ	normal stress	Pa
τ	torsional shear stress	Pa

Subscript

s	observed in the stationary frame
r	observed in the rotating frame
ax	axis

bp	base point
max	maximum
min	minimum
us	usage factor
n	normal
a	amplitude

REFERENCES

Adams G. P., "Modelling and computer simulation of rotor chatter and oscillating bearing forces in twin screw compressors", PhD. Dissertation, Purdue University, 1997.

Huagen, W., Yuan M., Ziwen X. "Theoretical and experimental investigation of compression loads in twin screw compressor", International Compressor Engineering Conference at Purdue, 2004. Paper 1701. DOI: https://docs.lib.purdue.edu/icec/1701

Inc., C. (2020). COMSOL. Retrieved from http://www.comsol.com/products/multiphysics/

Inc., R. V. A. (2022). Dyrobes. Retrieved from http://www.dyrobes.com/

Kliemann, Wolfgang, & Namachchivaya, N. S. (2017). Nonlinear Dynamics and stochastic mechanics. CRC Press.

Lee, C.-W., & Seo, Y.-H. (2009). Enhanced Campbell diagram with the concept of H∞ in rotating machinery: Lee Diagram. Journal of Applied Mechanics, 77(2). https://doi.org/10.1115/1.3173610

Lee, W. S., Ma, R. H., Wu, W. F., Chen, S. L., & Hsia, H. W. (1999). Performance and bearing load analysis of a Twin Screw Air Compressor. Journal of Mechanics, 15(2), 69–78. https://doi.org/10.1017/s1727719100000344

Muhammed, A. R., & Childs, D. W. (2013). Rotordynamics of a two-phase flow twin screw pump. Journal of Engineering for Gas Turbines and Power, 135(6). https://doi.org/10.1115/1.4023490

Patel, H. H., & Lakhera, V. J. (2019). A critical review of the experimental studies related to twin screw compressors. Proceedings of the Institution of Mechanical Engineers, Part E: Journal of Process Mechanical Engineering, 234(1), 157–170. https://doi.org/10.1177/0954408919869534

Stosic, N., Smith, I., & Kovacevic, A. (2005). Screw Compressors: Mathematical Modelling and Performance Calculation. Springer.

Svärd, H. (2015). A branch and bound algorithm for evaluation of the Findley Fatigue Criterion. International Journal of Fatigue, 73, 27–38. https://doi.org/10.1016/j.ijfatigue.2014.11.008

Zhou, Z., Wang, D., Zhu, T., & Mao, J. (1990). Analysis of the Applied Forces in Twin-Screw Refrigerant Compressors. Proceedings of the International Compressor Engineering Conference at Purdue, USA: p. 8~17

ACKNOWLEDGEMENT

The authors would like to thank Ingersoll Rand for the financial and technical support of this project.